AD-A089 042 SUSSEX UNIV BRIGHTON (ENGLAND) SCHOOL OF ENGINEERING--ETC F/G 11/6
THE AS-QUENCHED MICROSTRUCTURE AND TEMPERING BEHAVIOUR OF RAPID--ETC(U)
JUN 80 J J RAYMENT, B CANTOR N00014-78-G-0039
UNCLASSIFIED TR-9 NL

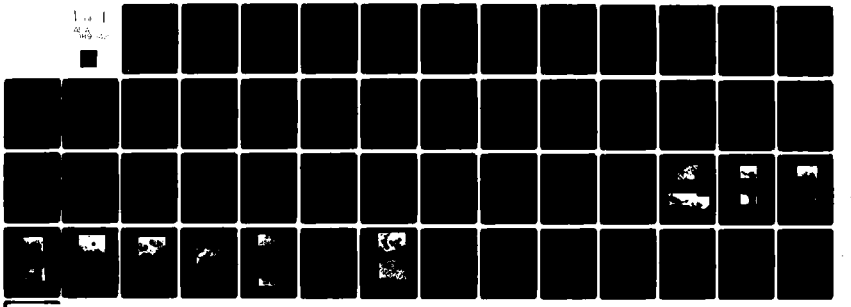

END
DATE FILMED
10-80
DTIC

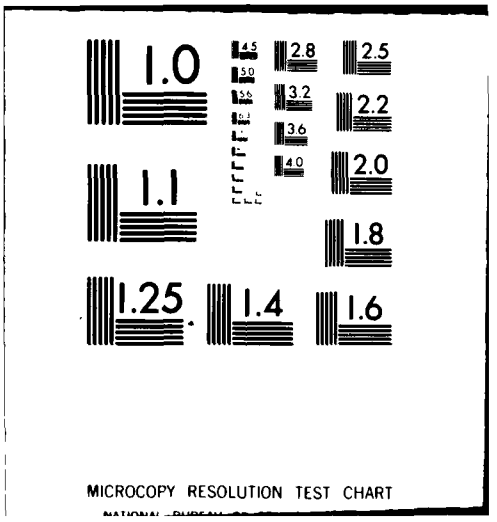
1.0
1.1
1.25
1.4
1.6
1.8
2.0
2.2
2.5
2.8
3.2
3.6
4.0
4.5
5.0
MICROCOPY RESOLUTION TEST CHART

AD A089042

DDC FILE COPY

SECURITY CLASSIFICATION OF THIS PAGE (When Data Entered)

REPORT DOCUMENTATION PAGE

READ INSTRUCTIONS BEFORE COMPLETING FORM

1. REPORT NUMBER: Technical Report No 9
2. GOVT ACCESSION NO.: AD-A089042
3. RECIPIENT'S CATALOG NUMBER: 9
4. TITLE (and Subtitle): The As-Quenched Microstructure and Tempering Behaviour of Rapidly Solidified Tungsten Steels.
5. TYPE OF REPORT & PERIOD COVERED: Technical Report
6. PERFORMING ORG. REPORT NUMBER:
7. AUTHOR(s): J.J. Rayment and B. Cantor
8. CONTRACT OR GRANT NUMBER(s): N00014-78-G-0039
9. PERFORMING ORGANIZATION NAME AND ADDRESS: School of Engineering and Applied Sciences, University of Sussex, Brighton, Sussex, U.K.
10. PROGRAM ELEMENT, PROJECT, TASK AREA & WORK UNIT NUMBERS:
11. CONTROLLING OFFICE NAME AND ADDRESS: Metallurgy Branch, Office of Naval Research, Arlington, VA 22217
12. REPORT DATE: 12th June 1980
13. NUMBER OF PAGES: 50
14. MONITORING AGENCY NAME & ADDRESS (if different from Controlling Office): TR-9
15. SECURITY CLASS. (of this report): Unclassified
15a. DECLASSIFICATION/DOWNGRADING SCHEDULE:
16. DISTRIBUTION STATEMENT (of this Report): Unlimited
17. DISTRIBUTION STATEMENT (of the abstract entered in Block 20, if different from Report):
18. SUPPLEMENTARY NOTES:
19. KEY WORDS (Continue on reverse side if necessary and identify by block number): Rapid-solidification, Tungsten Steels, Tempering, Transmission Electron Microscopy, Mechanical Properties
20. ABSTRACT (Continue on reverse side if necessary and identify by block number):

Transmission electron microscopy and microhardness testing were used to examine the as-quenched structure and mechanical properties of a series of iron-tungsten-carbon alloys ranging from 6 to 23 % tungsten with a constant W:C atomic ratio of 2:1 and T1 tool steel. The iron-tungsten-carbon alloys were found to exhibit a significant change in microstructure and hardness as the tungsten and carbon content were increased. The change in morphology was from lath martensite in the lower tungsten alloys

DD FORM 1 JAN 73 1473 EDITION OF 1 NOV 65 IS OBSOLETE S/N 0102-LF-014-6601

Unclassified

SECURITY CLASSIFICATION OF THIS PAGE (When Data Entered)

continued....

to a solidification structure of δ-ferrite cells surrounded by austenite and M_6C carbide, in the higher tungsten alloys. An increse in the hardness from 700 $kgmm^{-2}$ to 1050 $kgmm^{-2}$ accompanied this change in morphology. A model is proposed to explain the morphological change, In addition. the tempering behaviours of rapidly solidified Fe-6.3 wt%W-0.21wt%C, Fe-23wt%W-0.75wt%C and T1 tool steel were examined and compared to those observed for the conventional solution-treated and quenched alloys.

The As-Quenched Microstructure And Tempering Behaviour of Rapidly Solidified Tungsten Steels

by

J.J. Rayment and B. Cantor

School of Engineering & Applied Sciences
University of Sussex
Falmer, Brighton
Sussex, BN1 9QT
ENGLAND

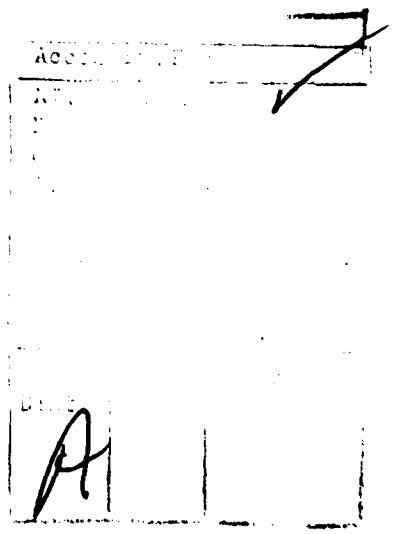

ABSTRACT

Transmission electron microscopy, and microhardness testing were used to examine the as-quenched structure and mechanical properties of a series of iron-tungsten-carbon-alloys ranging from 6 to 23 percent tungsten with a constant W:C atomic ratio of 2:1, and T1 high speed tool steel. The iron-tungsten-carbon alloys were found to exhibit a significant change in microstructure and hardness as the tungsten and carbon content was increased. The change in morphology was from lath martensite in the lower tungsten alloys to a solidification structure of δ-ferrite cells surrounded by austenite and M_6C carbide, in the higher tungsten alloys. An increase in hardness from 700 $kgmm^{-2}$ to 1050 $kgmm^{-2}$ accompanied this change in morphology. A model is proposed to explain the morphological change. In addition the tempering behaviours of rapidly solidified Fe-6.3wt%W-0.21wt%C, Fe-23wt%W-0.75wt%C and T1 high speed tool steel were examined and compared to those observed for the conventional solution-treated and quenched alloys.

INTRODUCTION

Rapid solidification, or as it is sometimes called, splat-quenching, has been a field of vigorous research activity in recent years, particularly in connection with metallic glasses. Lately, the rapid solidification of crystalline alloys has attracted increasing attention, especially in the case of iron-base alloys. The well known beneficial effects of rapid solidification, namely refinement of grain size, homogenisation of microstructure and extension of solid solubility, lend themselves well to typical microstructural problems found in conventional steels, such as an inhomogeneous microstructure with a coarse dispersion of carbides.

The present work describes an investigation by transmission electron microscopy (TEM) and microhardness testing into the effects of rapid solidification upon a series of six iron-tungsten-carbon alloys and a tungsten-based commercial high speed steel, AISI T1. The three main reasons for investigating the ternary Fe-W-C alloys as well as T1 were as follows.

1) T1 is essentially an iron-tungsten-carbon alloy with additions of vanadium to prevent grain growth during solution treatment, and chromium to provide hardenability on quenching. These two additions would appear to have no obvious function in a rapidly solidified steel where there is no solid-state solution treatment and where martensite is often suppressed during the rapid quenching.

2) Phase transformations in high speed steels are complex under equilibrium conditions and have been shown to be further complicated when metastable, rapid quenching effects are taken into account [1]. It was hoped that the iron-tungsten-carbon alloys would present similar, but less complex microstructures and mechanical properties for interpretation.

3) The isothermal tempering behaviour of solution-treated and brine-quenched Fe-6.3wt%W-0.21wt%C has been studied extensively [2]. Rapid solidification of this alloy would almost certainly result in a finer microstructure, and this might be expected to alter the isothermal tempering characteristics.

The iron-tungsten-carbon alloys ranged from 6.3wt% to 23wt% tungsten, with a constant tungsten:carbon atomic ratio of 2:1 (See Table 1). The Fe-23wt%W-0.75wt%C alloy was chosen to represent a simplified T1 steel, the carbon content being the same in both alloys, while the vanadium and chromium in T1 is replaced by additional tungsten in the ternary alloy. At the other end of the range of ternary alloys was the Fe-6.3wt%W-0.21wt%C alloy previously examined in the solid state [2]. The other four alloys were chosen to span the range between the two alloys mentioned above.

The effect of rapid solidification upon the microstructure and hardness of these ternary alloys as a function of composition was investigated and the relative isothermal tempering

behaviours of rapidly solidified and solid-state quenched Fe-6.3wt%W-0.21wt%C were compared. A preliminary investigation was also made of the relative isochronal tempering behaviours of rapidly solidified and solid-state quenched Fe-23wt%W-0.75wt%C and T1 tool steel.

EXPERIMENTAL PROCEDURE

Commercial grade T1 high speed tool steel was obtained in the form of 13mm diameter rod. The other alloys, shown in Table 1, were prepared from ≥ 99.99% pure iron, tungsten and carbon by induction melting in recrystallised alumina crucibles under a dynamic argon atmosphere. The as-cast alloys were homogenised for 100 hours at 1130°C and specimens were taken from the homogenised alloys for rapid solidification. Rapid solidification was achieved by means of a two-piston apparatus described previously [3]. Individual specimens of ∿ 0.7 gram mass were levitation melted in an argon atmosphere and then allowed to fall under gravity until quenched between two piston accelerated magnetically. The rapidly solidified foils were generally 70-120 μms in thickness and approximately 30mm in diameter. The effective cooling rate has been measured as ∿ 10^7 Ks^{-1} at the melting point, falling to ∿ 10^5 Ks^{-1} at 700°C [4].

In order to compare the structural and mechanical properties of the rapidly solidified alloys with solution treated and solid-state quenched alloys, specimens of the latter were

obtained by cold rolling the homogenised alloys ∿ 50 percent and then solution treating at 1150°C for 50 hours, followed by a brine quench. All heat treatments were carried out either in sealed silica capsules which had been evacuated and then flushed through with argon, or under a dynamic argon atmosphere. Microhardness testing was carried out using a Leitz microhardness tester with a Vickers diamond indenter. Rapidly solidified and solid-state quenched specimens were tested with 50 gram and 200 gram loads respectively. Thin foils were prepared for TEM by a jet polishing technique using a solution of 20 percent perchloric acid in methanol at ∿ -15°C. A JEM 100C (120kV) microscope was used for the electron microscopy.

RESULTS

The As-Quenched State

In rapidly solidified FeWC1-3, that is alloys containing up to 13wt% tungsten (see Table 1), the typical as-quenched microstructure was lath martensite, as seen in Fig 1. The dimensions of the martensite laths in the three alloys varied only slightly and were of the order of 0.1 - 0.3μm in width and 1 - 3.0μm in length.

In rapidly solidified FeWC4 alloy (16.5wt% tungsten) two types of microstructure were seen. In a few areas, a martensitic lath structure, similar to that seen in the lower

tungsten alloys was present, but in all other areas examined, a cellular, solidification structure was observed. An example of this cellular microstructure can be seen in Fig 2. The microstructure was found to consist of δ-ferrite cells, $\sim$0.6 - 1.0μm in diameter, surrounded by austenitic cell boundaries $\sim$ 0.05 - 0.1μm thick. Fig 2b is a selected area diffraction pattern (SAD) taken from the area shown in Fig 2a. Using $(110)_\alpha$ and $(111)_\gamma$ reflections for centred dark field microscopy (CDF) it was possible to illuminate areas within a cell and cell boundary respectively. (Fig 2 c-d).

In rapidly solidified FeWC5-6 (20 and 23wt% tungsten) only the cellular microstructure was observed, with δ-ferrite cells, 0.3 - 1.0μm in diameter. In this case, however, the cell boundaries were found to contain not only austenite but also M_6C carbide. Figs 3 and 4 show the cellular microstructure of the higher tungsten alloys. Selected area diffraction of the area shown in Fig 4a revealed $[00\bar{1}]_\gamma$ and $[01\bar{2}]_{M_6C}$ zones with the orientation relationship.

$$(110)_\gamma \;||\; (100)_{M_6C}$$
$$(010)_\gamma \;||\; (\bar{2}2\bar{1})_{M_6C}$$

Using a $(\bar{2}4\bar{2})_{M_6C}$ reflection, the CDF image shown in Fig 4b was obtained. The carbide can clearly be seen to exist in the cell boundaries. In general, there did not appear to be a unique relationship between the austenite and M_6C carbide in the rapidly solidified alloys. Indeed, many different

orientation relationships were observed. Figure 5 shows the microhardness of rapidly solidified and solid-state quenched Fe-W-C alloys as a function of tungsten content. All the solid-state quenched Fe-W-C alloys had microhardness values in the range 750-800 $kgmm^{-2}$. Rapidly solidified FeWC1 and 2 (6.3 and 9.5wt% tungsten) had microhardness values of $\sim$ 700 $kgmm^{-2}$, not very different from the solid-state quenched alloys. However, in FeWC4-6 (16.0 - 23.0wt% tungsten), the as-quenched hardness was much greater, $\sim$ 1050 $kgmm^{-2}$.

As with FeWC5 and 6 (20 and 23wt%W) the as-quenched microstructure of rapidly solidified T1 tool steel was found to consist of δ-ferrite cells surrounded by cell boundaries containing austenite and M_6C carbide. The cell dimensions were similar to those observed in rapidly solidified FeWC5 and 6 alloys, and an example of the cellular microstructure is shown in Fig 6. The hardness of rapidly solidified T1 tool steel was 615 $kgmm^{-2}$, in comparison to a hardness of $\sim$ 800 $kgmm^{-2}$ found in the commercial alloy quenched from the solid-state.

The Tempering of Fe-6.3wt%W - 0.21wt%C:

Fig 7 shows the effect of isothermal tempering at 600^{o}C on the microhardness of both rapidly solidified and solid-state quenched FeWC1 (6.3wt%W). The tempering behaviour of rapidly solidified and solid-state quenched specimens was almost

identical. In each case the as-quenched hardness of 700-800 $kgmm^{-2}$ fell abruptly to 450-470 $kgmm^{-2}$ after 1 hour at $600^{o}C$. This drop in hardness was followed by a small secondary hardening peak, with a peak hardness of 475-500 $kgmm^{-2}$ after 2-3 hours, and then eventual overaging at times greater than 5 hours.

Specimens of rapidly solidified FeWCl (6.3wt%W) tempered at $600^{o}C$ for 40 minutes, 10 hours and 50 hours were chosen for examination by TEM. These three specimens were picked to represent the initial softening, secondary hardening and overaging periods respectively. Transmission electron microscopy of rapidly solidified FeWCl, tempered at $600^{o}C$ for 40 minutes showed that the initial lath martensite structure was retained, but within the laths there was a Widmanstätten array of precipitates identified as cementite (Fe_3C), see Fig 8. The cementite exhibited the Bagaryatski orientation relationship with the tempered martensite in agreement with the results obtained by Davenport [2], namely,

$$\{110\}_{\alpha} \;||\; (100)_{Fe_3C}$$

$$\langle 110\rangle_{\alpha} \;||\; [01\bar{0}]_{Fe_3C}$$

After tempering at $600^{o}C$ for 10 hours, specimens of rapidly solidified FeWCl were found to contain a fine-scale precipitation on interlath and prior austenite grain boundaries and to a lesser extent, within the laths. Those precipitates which could be identified were W_2C carbides and the orientation

relationship between W_2C and the tempered martensite was found to be consistent with that observed by Dyson et al [5] for Mo_2C in ferrite namely

$$(110)_\alpha \;||\; (00.1)_{W_2C}$$
$$[100]_\alpha \;||\; [2\bar{1}.0]_{W_2C}$$

Whether there was still any cementite present could not be positively verified by either bright-field imaging or by selected area diffraction. A specimen of the tempered alloy was therefore further examined by a combination of scanning-transmission electron microscopy (STEM), scanning secondary electron microscopy (SEM) and X-ray analysis by energy dispersive spectroscopy (EDS) in a JEM 100C TEMSCAN microscope. The SEM and STEM micrographs of one of the regions examined are shown in Fig 9. The areas chosen for element micro-analysis were (i) individual carbide particles visible in both SEM and STEM, points 1 - 7, and (ii) areas within the matrix that appeared to be free of any carbides, points 8 and 9. Table II lists the $W_{M\alpha}/Fe_{K\alpha}$ ratios for the individual points. These ratios show the existence of two types of carbide; one with a significant tungsten content as found at point 1, the other with little or no tungsten content at all, as found at point 4. The matrix was found to contain very little tungsten. The nature of elements present in tool steel carbides is relatively well known [6]. In M_3C carbide, the metallic element is predominantly iron and the carbide can dissolve only a little tungsten, whereas M_2C is a tungsten-

rich carbide. From this evidence, it is likely that the tungsten-rich carbide was indeed W_2C, and the carbide containing little or no tungsten was undissolved Fe_3C. There appeared to be no difference in morphology between the two types of carbide, and the relatively coarse cementite was found only at interlath boundaries, alongside W_2C precipitates.

After tempering at 600°C for 50 hours, rapidly solidified FeWCl contained blocky precipitates along interlath and prior austenite boundaries, and to a lesser extent, precipitates within the tempered laths. The blocky precipitates were identified as M_6C carbides and the precipitates within the laths were undissolved W_2C carbides. Electron diffraction patterns of M_6C and tempered martensite were consistent with either a Kurdjomov-Sachs relationship,

$$(011)_\alpha \;||\; (\bar{1}\bar{1}1)_{M_6C}$$
$$[1\bar{1}1]_\alpha \;||\; [01\bar{1}]_{M_6C}$$

or with a Nishiyama-Wasserman relationship

$$(011)_\alpha \;||\; (\bar{1}\bar{1}1)_{M_6C}$$
$$[01\bar{1}]_\alpha \;||\; [112]_{M_6C}$$

The ambiguity is not surprising considering that the two relationships differ by only 5°16'.

The Tempering of Fe-23wt%W - 0.75wt%C and T1 High Speed Steel:

Fig 10 shows the effect of isochronal tempering on the microhardness of rapidly solidified and solid-state quenched FeWC6 and T1 tool steel. The conventional solid-state quenched T1 tool steel showed a softening at $\sim 300^{o}C$, followed by a secondary hardening peak of ~ 950 kmm^{-2} at $\sim 530^{o}C$. In rapidly solidified T1, a large scatter in the hardness measurement at the lower temperatures made it difficult to determine if any softening had occurred. However a large secondary hardening peak was observed at $\sim 650^{o}C$ with a peak hardness of ~ 1050 kgmm^{-2}. There was no obvious secondary hardening in the solid-state quenched FeWC6. The as-quenched hardness of ~ 800 kgmm^{-2} dropped gradually to ~ 650 kgmm^{-2} at $500^{o}C$ and then further decreased to ~ 400 kgmm^{-2} at $650^{o}C$. The curve for the rapidly solidified alloy, on the other hand, showed an initial softening at $350^{o}C$, and then a secondary hardening of ~ 1000 kgmm^{-2} at $\sim 600^{o}C$ followed by overaging at higher temperatures.

The effect of tempering on the microstructure of rapidly solidified FeWC6 and T1 was not examined in full detail, but TEM studies showed that in FeWC6, cementite precipitation occurred at 300-$500^{o}C$, followed by M_6C precipitation within the cells at $\sim 650^{o}C$. In addition a significant proportion of the austenite in the cell walls transformed to bcc-iron by 550-$650^{o}C$, although it was not possible to identify positively the bcc phase, see Fig 11. During the tempering

of T1, there was little change in microstructure until 615°C, where fine M_2C needles were precipitated within the ferrite cells. This corresponded to the peak hardness. The precipitation of M_2C, as shown in Fig 12, was much finer than the M_6C precipitation observed in the tempered FeWC6 alloy. The majority of the austenite was still present after tempering at 615°C.

DISCUSSION

The As-Quenched Structure

The as-quenched microstructure of rapidly solidified FeWC1-3 is essentially fine-scale lath martensite. The martensitic nature of FeWC1 is not surprising, as it has been shown previously that solid-solution treatment of the same alloy is capable of taking all the carbides into solution, and producing a martensitic structure on quenching [2]. The rapidly solidified microstructure, however, is 5-10 times finer than that obtained in the solid-state quenched alloy. The alloy systems Fe-4wt%Mo-0.2wt%C [7], Fe-2wt%V-0.2wt%C [7] and Fe-9wt%Cr-0.2wt%C [8] (all having a similar atomic composition to FeWC1) have also been shown to form a fully martensitic as-quenched structure after suitable solution treatments in the solid-state. In addition, one of these alloys, Fe-4%Mo-0.2%C, has been examined after rapid solidification by Sare [9] using a gun technique which gave specimens of varying thickness. In thin, electron transparent regions, Sare found δ-

ferritic grains elongated in the plane of the foil but was not able to detect any martensite. In slower-cooled, thick regions, however, the structure was mainly finely-twinned martensite, with some retained high temperature ferrite. The estimated cooling rate for the gun rapid-quencher is 10^6-10^8 Ks^{-1} [10], in comparison to 10^5-10^7 for the two-piston apparatus used in this investigation. Therefore the fact that δ-ferrite is present in splat-quenched Fe-4wt%Mo-0.2wt%C and not in Fe-6.3wt%W-0.21wt%C is probably a consequence of the different rates of cooling. A more detailed discussion of the effect of cooling rate on microstructure is presented in the next section.

The microstructures of rapidly solidified FeWC2 and 3 differ from those obtained for the solution-treated/brine-quenched alloys. In the former there is complete solid solubility, whereas the latter alloys have been shown previously to contain significant amounts of M_6C carbide with the carbide content increasing with alloy content [11,12]. The primary effect of rapid solidification on iron-tungsten-carbon alloys containing up to 13wt% tungsten, is therefore, to produce a fine scale martensitic microstructure with complete solution of alloying elements.

The cellular microstructure observed in the higher tungsten, rapidly-solidified alloys (> 13wt%W) is not observed in the corresponding solid-state quenched alloys where it has been previously shown that the only phases present are bcc-iron,

identified by optical microscopy as martensite, and M_6C carbide [11,12]. The as-quenched microstructure of rapidly solidified T1 tool steel is also different from that observed in the conventionally treated alloy which has been found to be a severely cored structure of predominantly martensite with austenite, M_6C carbide and possibly a little retained δ-ferrite [6]. The amount of carbide present in both solid-state quenched FeWC4-6 and in T1 tool steel is significantly higher than that detected in the rapidly solidified alloys. The non-martensitic cellular microstructure of rapidly solidified FeWC4-6 and T1 is, therefore, very different from the structures seen in the solution-treated and quenched alloys.

The Effect of Cooling Rate on Rapidly Solidified High Speed Tool Steels

Several investigations into the rapid solidification high-speed steels have shown different as-quenched microstructures. The results of these experiments are summarised in Table III. The differences in the structure of high speed tool steels obtained on rapid solidification can be explained as the result of different rates of cooling. The investigations by Arai and Komatsu [13,14] and Niewiarowski and Matyja [15] almost certainly used relatively low cooling rates. In the results obtained by Arai and Komatsu, the microstructure was primary γ and eutectic γ and carbide, with ferrite found only in a few areas, and in the results of Niewiarowski and Matyja, the bcc phase was not properly identified but from

X-ray and hardness data it was probably either martensite or a mixture of martensite and δ-ferrite. In the investigations by Jama and Thursfield [16], Tuli et al [17,18] and Sare[1], higher cooling rates were obtained, and the δ-ferrite phase was found in large quantities in the rapidly solidified material. Jama and Thursfield [16] found δ-ferrite close to the foil surface, while in the work of Tuli et al [17,18], the δ-ferrite existed as cells surrounded by regions of austenite, M_2C and $M_{23}C_6$ carbide. In the work by Sare [1], δ-ferrite was found in unthinned regions (which were assumed to be the fastest cooled) in the form of elongated dendrites and also as dendrites with inter-dendritic carbide precipitation. Austenite was found only in the thicker regions which were presumably cooled more slowly.

It is obvious that the rate of cooling has a strong effect on the rapidly solidified microstructure of high speed tool steels. As the rate of cooling is increased from conventional levels of 10^3 Ks^{-1}, through the lower end of rapid solidification rates, 10^5 Ks^{-1}, to the higher rates of 10^7-10^8 Ks^{-1} austenite and then in turn, δ-ferrite becomes increasingly stabilised. From the microstructural evidence obtained by electron microscopy and from the recently measured cooling rate of $\sim$ 10^7 Ks^{-1} achieved by the two-piston, splat-quencher [4], it would appear that the present work lies between the experimental results of Tuli et al [17,18] and that of Sare [1], on the scale of increasing cooling rate, and is in reasonably good agreement with the previous results.

In the present investigation, the as-quenched microstructure of rapidly solidified T1 tool steel is similar to laser-glazed microstructures obtained by Tuli et al [17,18], but there seems to be a disagreement about the type of carbide present. With electron diffraction of extraction replicas, Tuli suggested that the carbides in the cell walls are predominantly M_2C with some $M_{23}C_6$, whereas in the present investigation the carbide has been identified as M_6C. However, it is difficult to differentiate between $M_{23}C_6$ and M_6C because of the similarity in the electron diffraction patterns for these types of carbides; $M_{23}C_6$ has an fcc structure and M_6C has an fcc diamond structure, and the lattice parameters are 10.621Å and 11.08Å respectively. Although neither investigation has determined conclusively which of the carbides is present, M_6C is more likely, because it is the more common solidification carbide. It may appear that the present investigation is in disagreement with previously reported results in which the microstructures of rapidly solidified tool steels were shown to be predominantly austenite [27]. In the previous reports, however, the microstructure was determined by X-ray diffractometry of the whole foil, whereas in the present investigation, the structure was determined by TEM from the central faster-cooled regions of the foil.

The Change in Morphology in Rapidly Solidified Iron-Tungsten-Carbon Alloys and T1 Tool Steel

The conventional solidification and cooling sequences of

FeWC1-6 alloys and T1 [19] tool steel are shown in Table IV. The solidification data for iron-tungsten-carbon alloys was obtained from binary sections of the ternary phase diagram constructed by Takeda[20] in the 1930's. In all the alloys, the peritectic reaction rarely goes to completion, even at relatively slow rates of cooling, and the remaining melt either transforms to supersaturated austenite (in alloys FeWC1-2) or transforms eutectically to austenite and M_6C carbide (in alloys FeWC3-6). On further cooling the δ-ferrite decomposes to austenite which eventually transforms to martensite. The solidification carbide, M_6C forms at different stages of cooling, depending on the alloy composition. In FeWC1-2, M_6C precipitates from the supersaturated austenite, and in FeWC3-4, it precipitates eutectically from the melt. Only in FeWC5-6 does M_6C carbide form at the early stages of solidification, from the peritectic reaction.

Rapidly solidified iron-tungsten-carbon alloys show a dramatic change in structure at 13-16.5wt% tungsten. Below this tungsten content, the as-quenched structure is martensitic, but at higher tungsten content, the structure is cellular, δ-ferrite with austenite and M_6C carbide in the cell boundaries. In rapidly solidified FeWC1-3($\leq$13wt% tungsten), the martensitic microstructure indicates that the solidification reactions undergone during quenching are those shown in Table IV. In these alloys, precipitation of M_6C carbide from the supersaturated austenite is completely suppressed. In rapidly solidified FeWC4 (16.5wt% tungsten) the cellular microstructure

of δ-ferrite and austenite indicates that solidification proceeds only as far as the peritectic formation of austenite. The eutectic reaction and all subsequent solid-state transformations are suppressed. In rapidly solidified FeWC5-6 (>16.5wt% tungsten) the solidification reactions are the same as shown for FeWC4, but with M_6C as well as austenite produced by the peritectic transformation. Because of the similarities between the rapidly solidified microstructure and the phase diagrams of T1 tool steel and FeWC6 alloy, the solidification reactions under rapid solidification conditions are assumed to be the same.

Increasing the alloy content in rapidly solidified iron-tungsten-carbon alloys leads to the retention of δ-ferrite. It would appear, therefore, that tungsten which as a bcc alloying element is a known ferrite stabiliser [6] has overcome the effect of carbon, an austenite stabiliser. What are not obvious are the factors that determine the critical alloying content, above which δ-ferrite is stabilised, but below which the δ-ferrite decomposes to austenite and then martensite on cooling.

Fig 13 shows the equilibrium temperatures of (i) the $\delta \rightarrow \gamma$ transformation, and (ii) the start of the $\gamma \rightarrow \alpha$ transformation as a function of tungsten content in iron-tungsten-carbon alloys. The data was taken from the iron-tungsten-carbon binary sections by Takeda [20]. It can be seen that increasing the tungsten (and carbon) content effectively decreases the

region of austenite stability by a combination of (a) lowering the $\delta \rightarrow \gamma$ transformation temperature and (b) raising the $\gamma \rightarrow \alpha$ transformation temperature.

The $\delta \rightarrow \gamma$ transformation can occur by either a diffusional or diffusionless process. Since the first type of process requires time for the diffusing elements to travel, often it will only be reactions that require diffusion to occur over short distances that actually proceed. If insufficient time for diffusional transformation is available, then it is possible for the $\delta \rightarrow \gamma$ transformation to occur diffusionlessly. This type of reaction will particularly be favoured with large degrees of undercooling. From the temperature range of austenite stability shown in Fig 13 and from the estimated rate of cooling, it is possible to calculate the time available for a diffusional $\delta \rightarrow \gamma$ transformation before the ferrite phase becomes stable once more. With the time known, and the appropriate diffusivities of tungsten and carbon in δ-ferrite estimated, it is possible to determine on what scale a diffusional transformation could occur. Tables V and VI show the estimated diffusion coefficients of tungsten and carbon in δ-ferrite, the time available for the $\delta \rightarrow \gamma$ transformation and the subsequent diffusion distances. The diffusion coefficients were obtained by extrapolating data for α-ferrite, at the mean temperature between the $\delta \rightarrow \gamma$ and $\gamma \rightarrow \alpha$ transformation temperatures. The transformation time available was estimated by dividing the temperature range by the measured cooling rate for the mean temperature.

The distances diffusing elements could travel in the available time was then calculated from the well known equation [21],

$$X = \sqrt{Dt}$$

as shown in the tables. Tables V and VI show that if only the diffusion of carbon is considered necessary for the $\delta \rightarrow \gamma$ transformation to occur, then the transformation is unlikely because the diffusional distance is small in comparison to the δ-ferrite cell size ($\sim$ 0.5 - 1.0 μm), assuming that nucleation of austenite is difficult within the cell and that the austenite forms by the growth of existing austenite at the cell boundaries. Moreover, if diffusion of tungsten is considered necessary as well, then the diffusional transformation is surely not possible.

The as-quenched microstructure of the iron-tungsten-carbon alloys shows that in the alloys containing up to and including 13wt% tungsten a $\delta \rightarrow \gamma$ transformation (and subsequent $\gamma \rightarrow \alpha'$ transformation) did occur. Therefore the $\delta \rightarrow \gamma$ transformation must have been a diffusionless transformation. If a transformation is diffusionless, then the composition of both phases is fixed and the free energy of each phase depends only on the temperature. For the diffusionless transformation to occur, the transformation temperature must be lower than T_o, the equilibrium temperature at which the free energies of both phases are the same. In assessing the $\delta \rightarrow \gamma'$ transformation (the prime indicates that γ is of the same

composition as the δ), the undercooling required can be assumed to be similar to the undercooling for the well known $\gamma \rightarrow \alpha'$ transformation. This is not an unreasonable assumption; in Fe-29%Ni, a $\alpha \rightarrow \gamma'$ spontaneous transformation can occur on heating. This bcc to fcc transformation is diffusionless with a superheating almost identical to the undercooling required for the reverse $\gamma \rightarrow \alpha'$ reaction. In the case of the $\gamma \rightarrow \alpha'$ martensite transformation, the reaction requires a significant undercooling below T_o because the free energy change for the reaction, must overcome the surface energy of the newly formed plates and the elastic strain energy. In iron-carbon alloys, the undercooling needed has been found to be $\sim 200^{o}C$, and is almost independent of composition [22]. It is probable that a similar undercooling is required for iron-tungsten-carbon alloys. In rapidly solidified alloys, however, the undercooling would be further increased by:

i) a small austenite grain size, which has been shown to depress the Ms temperature of rapidly solidified iron-nickel alloys by as much as $200^{o}C$ [23] and

ii) an increased solubility of alloying elements in the austenite phase of rapidly solidified steels, leading to a depression of the Ms temperature.

A similar Ms depression is likely to occur in the rapidly solidified Fe-W-C alloys, although possibly not as large as that seen in the Fe-Ni alloys. In addition, the increased solubility of tungsten in the rapidly solidified Fe-W-C alloys, would produce a larger Ms depression in the higher

tungsten alloys then in the lower tungsten alloys. Taking both effects into account the undercooling required for the $\gamma \rightarrow \alpha'$ transformation in rapidly solidified iron-tungsten-carbon alloys is assumed to be 300°C for FeWC1-4 and 350°C for FeWC5-6.

The $\gamma \rightarrow \alpha'$ (martensitic) transformation in steels is a well known reaction. At the temperatures where this reaction commonly takes place (600-200°C) even conventional brine quenching is too fast to allow diffusional transformation to take place. A diffusionless $\delta \rightarrow \gamma'$ transformation is not so well known because at temperatures where this reaction would occur (> 1300°C) diffusion is normally fast enough for the diffusional reaction to take place readily. Only when cooling rates in excess of 10^6 Ks^{-1} are achieved, would there be the possibility of suppressing the diffusional reaction and allowing the diffusionless reaction to occur instead.

In Fig 13 the equilibrium $\delta \rightarrow \gamma$ and $\gamma \rightarrow \alpha$ transformation temperatures are shown as functions of tungsten content. Also included in the diagram are the following:

(i) The T_o temperatures for the $\delta \rightarrow \gamma'$ transformation; these values were estimated from Takeda's binary phase diagrams by taking the mid-point of the $\gamma + \delta$ region for each composition.

(ii) The A_g temperatures for the $\delta \rightarrow \gamma'$ diffusionless transformation; the undercoolings required were taken as 300°C

for the low tungsten alloys rising to 350°C for the FeWC5-6 alloy.

iii) The M_s temperatures for the $\gamma \rightarrow \alpha'$ martensitic transformation; these will be discussed below.

At tungsten contents corresponding to rapidly solidified alloys FeWC1-3, the estimated A_s temperatures, for the start of the diffusionless transformation of $\delta \rightarrow \gamma'$ lie above the corresponding temperatures for the start of the equilibrium $\gamma \rightarrow \alpha$ transformation, and are therefore in the region where austenite is stable. This means that the diffusionless transformation of $\delta \rightarrow \gamma'$ can take place. At the tungsten contents corresponding to rapidly solidified FeWC4-6, however, the A_s temperatures are below the $\gamma \rightarrow \alpha$ transformation temperatures, and are in the region where ferrite is once more stable. It is therefore unlikely that the $\delta \rightarrow \gamma'$ transformation will occur in these alloys. This explains why the as-solidified δ-ferrite in FeWC4-6, when not consumed by the peritectic reaction, does not transform to γ or γ' on cooling and is retained to room temperature.

In rapidly-solidified FeWC4-6 the as-solidified peritectic austenite is also retained to room temperature. In order to try and see why this should happen it is necessary to find out how the M_s temperature varies with alloy content. The M_s temperature for FeWC1 is estimated to be 378°C from the following equation for low alloy steels [24].

$$M_s(^oC) = 561 - 474(\%C) - 33(\%Mn) - 17(\%Ni) - 17(\%Cr) - 13(\%W)$$

The M_s temperature for T1 tool steel, and therefore approximately FeWC6, is known to be 220°C [6]. The other M_s temperatures can be estimated by looking at known M_s temperatures for iron-carbon alloys [25] using the M_s values for FeWC1 and 6 as limits. All these values are then lowered by 100-150°C to take into account the effect of rapid solidification which, as mentioned previously, has been shown to depress the M_s temperature. These estimated M_s temperatures are plotted in Fig 13. The M_s temperature falls from 573K for FeWC1 to 343K for FeWC6. The martensite transformation is therefore possible in all alloys, but is perhaps at too low a temperature to occur in FeWC4-6.

The As-Quenched Hardness

The hardness results of rapidly solidified iron-tungsten-carbon alloys and T1, are on the whole, difficult to explain, and it has not been possible to achieve a good interpretation.

The as-quenched hardness of rapidly solidified iron-tungsten-carbon alloys shows a significant increase when the microstructure changes from martensite to cellular ferrite. In the martensitic alloys, the hardness is $\sim$ 700 - 750 $kgmm^{-2}$, while in the cellular ferritic alloys, the hardness is 1050 - 1100 $kgmm^{-2}$. This is surprising as ferrous martensites are generally hard alloys with high dislocation densities whereas ferrite is usually a relatively soft phase. There are, four

effects that might be considered possible causes of the high hardness of the ferritic alloys;

(i) Autotempering may have occurred in the martensite during cooling. There was no evidence of this, however, in transmission electron microscopy.

ii) A high hardness might be expected if the δ-ferrite cells were much smaller than the martensite plates. This however, was not the case.

iii) The δ-ferrite may have contained a high dislocation density as a result of being squeezed between two fast-moving pistons. However, this would apply equally to the martensite and therefore cannot be the reason for the significant difference in hardness.

iv) Solid solution hardening would have increased with increasing tungsten content and may become a significant effect in the δ-ferritic alloys. This has not been confirmed, but is quite probable.

Rapidly solidified and solid-state quenched FeWC1 (6.3wt% tungsten) have almost the same as-quenched hardness of approximately 750 $kgmm^{-2}$. The as-quenched hardness of the same solid-state quenched alloy as studied by Davenport [2] was $\sim$ 500 $kgmm^{-2}$. It is possible that this difference is related to a difference in martensite lath dimensions. Recent work by Duflos and Cantor [26] on rapidly solidified pure iron, has shown that a small martensite lath or plate size can lead to a very high hardness by a Hall-Petch effect. The martensite lath dimensions for the rapidly solidified

and solid-state quenched FeWC1 alloy are typically ∿ 2 μm in length and ∿ 0.2 - 0.5 μm in width (rapidly solidified) and 10-15 μm in length and ∿ 1.0 μm in width (solid-state quenched). This compares to the typical lath dimensions of ∿ 30 μm and ∿ 2.0 μm seen in Davenport's alloy [2]. It is difficult to explain why the rapidly solidified and solid-state quenched hardnesses of FeWC1 are so similar when the rapidly solidified microstructure is five times finer. The difference between the hardness of the solid-state quenched alloys of the present investigation and of Davenport's [2], however, may be a direct consequence of a finer microstructure produced by a faster, more efficient brine quench.

The hardnesses of rapidly solidified FeWC6 and T1 tool steel are ∿ 1050 $kgmm^{-2}$ and ∿ 600 $kgmm^{-2}$ respectively. There is no obvious reason for the difference, as the as-quenched microstructures are essentially the same and of similar dimensions. In addition, neither alloy appears to have undergone carbide precipitation during quenching.

The Tempering of Rapidly Solidified Fe-6.3wt%W-0.21wt%C

The tempering sequence in rapidly solidified Fe-6.3wt%W-0.21wt%C is as follows

$$Fe_3C \rightarrow W_2C \rightarrow M_6C$$

The appearance of Fe_3C after 40 minutes at 600°C coincides with

a drop in hardness from $\sim$ 750 to $\sim$ 470 $kgmm^{-2}$. After 10 hours at 600°C, precipitation of W_2C carbide has occurred, although some cementite has remained in the form of coarse particles on lath and grain boundaries; the hardness has risen and there is a secondary hardening peak, with a hardness of $\sim$ 500 $kgmm^{-2}$. After 50 hours at 600°C, M_6C carbide precipitation is well established and produced a drop in hardness to $\sim$ 400 $kgmm^{-2}$, although some W_2C carbide is still present.

In comparison a very similar tempering sequence for Fe-6.3wt%W-0.23wt%C solution treated and brine-quenched was found by Davenport [2] to be:-

at grain boundaries $Fe_3C \rightarrow W_2C + M_{23}C_6 \rightarrow M_6C + M_{23}C_6$

within the matrix $Fe_3C \rightarrow W_2C \rightarrow M_6C$

$\searrow\ M_{23}C_6 \rightarrow M_6C$

Davenport observed that the $Fe_3C \rightarrow W_2C$ reaction did not go to completion. Instead the unconsumed cementite transformed to $M_{23}C_6$ probably by nucleation on the cementite/ferrite interface. It may be that a similar precipitation occurs in rapidly solidified and tempered FeWCl, but as mentioned previously, it is not easy to differentiate conclusively between M_6C and $M_{23}C_6$ carbides.

In addition to the tempering of rapidly solidified FeWCl, the present investigation includes the tempering of solution treated and brine-quenched FeWCl. The solid-state quenched

alloy displays a very similar tempering curve to that observed for the rapidly solidified alloy, although with a hardness generally 20-30 $kgmm^{-2}$ lower. It is however, $\sim$ 50 $kgmm^{-2}$ higher than the tempering curve reported by Davenport [2]. The most likely reason for this difference is that the quench obtained in the present investigation is faster and produces a finer, harder microstructure (see last section).

The Tempering of Rapidly Solidified Fe-23wt%W-0.75wt%C and T1 High Speed Tool Steel

During the isochronal tempering of rapidly solidified Fe-23wt%-0.75wt%C M_6C carbide precipitates in the ferrite cells whereas during the tempering of rapidly solidified T1, M_2C carbide precipitates. The difference in the type of carbide may possibly be due to the presence of vanadium and chromium in the high speed tool steel. It was observed that during the tempering of rapidly solidified FeWC6, a significant amount of the austenite had transformed to bcc-iron at 550-650^{o}C, whereas in the rapidly solidified T1, the majority of austenite was retained. During tempering, the austenite present in the cell boundaries of FeWC6 may have transformed isothermally to ferrite and cementite, however, the presence of vanadium and chromium in T1 effectively retarded this transformation and only a small amount of austenite decomposed.

In rapidly solidified FeWC6 and T1, the isochronal tempering curves show a hardening peak at higher temperatures and higher hardnesses than observed in the conventional solid-state

quenched alloys. This effect is stronger in T1, where the shift in the hardness peak to higher hardness and temperature is greater than the equivalent shift in FeWC6. The increase in peak hardness for the rapidly solidified alloys is presumably a consequence of the fine-scale of the precipitation. The higher hardness of T1 than that of $FeWC_6$ is almost certainly due to the different type of carbide formed during tempering and also because of the finer scale of precipitation in T1 than in $FeWC_6$. The higher peak temperatures of both rapidly solidified alloys has been caused by a delay in the onset of M_2C precipitation, but what effect has produced this delay is not known.

CONCLUSIONS

The following conclusions can be drawn from the investigation into the effect of rapid solidification on iron-tungsten-carbon alloys and T1 high speed steel.

1) Rapid solidification of iron-tungsten-carbon alloys containing less than or equal to 13wt% tungsten ($\leq$ 0.42wt%C) produces a fine martensitic lath microstructure.
2) Rapid solidification of iron-tungsten-carbon alloys containing 16.5wt% tungsten (0.54wt%C) produces a microstructure mainly of δ-ferrite cells surrounded by austenite cell boundaries but with some small areas where there is a martensitic lath structure, similar to that seen in the lower tungsten alloys.

3) Rapid solidification of iron-tungsten-carbon alloys containing greater than 16.5wt% tungsten (0.54wt%C) and up to 23%wt tungsten (0.75wt%C) produces a solidification microstructure of δ-ferrite cells surrounded by cell boundaries of austenite and M_6C carbide.

4) The iron-tungsten-carbon alloys which are martensitic on rapid solidification have a hardness of $\sim$ 700 $kgmm^{-2}$, whereas the alloys which are cellular ferritic on rapid solidification have a hardness of $\sim$ 1050-1100 $kgmm^{-2}$. This is difficult to explain but may be a consequence of solid-solution strengthening.

5) Rapid solidification of T1 high speed steel produces a solidification microstructure of δ-ferrite cells surrounded by cell boundaries of austenite and M_6C carbide. The structure is essentially the same as seen in the high tungsten ternary alloys (> 16.5wt% tungsten).

6) The as-quenched microstructure of rapidly solidified high speed steels is very dependent on the rate of cooling. At cooling rates of $\sim 10^8$ Ks^{-1}, the structure is almost entirely δ-ferrite. At slightly lower cooling rates of $\sim 10^6$-10^7 Ks^{-1}, as obtained in the present investigation, δ-ferrite cells are retained to room temperature but are surrounded by a region of austenite and carbide (either M_6C or M_2C). At even lower cooling rates ($\sim 10^5 Ks^{-1}$) almost no δ-ferrite is retained, and the microstructure is austenite with possibly some martensite. As the cooling rate reaches conventional levels (i.e. $\sim 10^3$ Ks^{-1}) the microstructure is predominantly martensitic with a little

retained austenite, with large quantities of as-solidified carbide.

7) There is a critical alloy content in iron-tungsten-carbon alloys, above which δ-ferrite is retained but below which the $\delta \rightarrow \gamma$ and subsequent $\gamma \rightarrow \alpha'$ transformations occur. It is probable that the diffusional $\delta \rightarrow \gamma$ transformation is too slow to occur in any of the rapidly solidified alloys. Instead, in alloys containing less than 16.5wt% tungsten a diffusionless $\delta \rightarrow \gamma'$ transformation occurs; in these alloys the estimated A_s temperatures lie in the region of austenite stability and above the region of α-ferrite stability. In rapidly solidified alloys containing ≥ 16.5wt% tungsten, however, the estimated A_s temperatures lie below the region of austenite stability and therefore in the region of ferrite stability. The diffusionless $\delta \rightarrow \gamma'$ transformation does not occur and δ-ferrite and the peritectic austenite and carbide are retained to room temperature.

8) The isothermal tempering behaviour of rapidly solidified Fe-6.3wt%W-0.21wt%C at 600°C is very similar to the alloy quenched from the solid-state with the following precipitation sequence

$$Fe_3C \rightarrow W_2C \rightarrow M_6C$$

The precipitation of Fe_3C is accompanied by a drop in hardness from 750-470 $kgmm^{-2}$. The onset of secondary hardening with a peak hardness of ∿ 500 $kgmm^{-2}$ corresponds

to the precipitation of W_2C carbide. Overaging follows, and the formation of M_6C carbide produces a gradual drop in hardness.

9) During the isochronal tempering of rapidly solidified Fe-23wt%W-0.75wt%C and T1 high speed tool steel, Fe_3C and M_6C precipitates in the former while M_2C precipitates in the latter. The presence of chromium and vanadium in rapidly solidified T1 appears to modify the precipitation process compared to rapidly solidified Fe-23wt%W-0.75wt%C.

10) The isochronal tempering curves for rapidly solidified Fe-23wt%W-0.75wt%C and T1 show a secondary hardening peak at higher temperatures and higher hardnesses than observed for the conventional solution-treated and quenched alloys. The higher peak hardnesses of the rapidly solidified alloys are probably the result of a much finer scale of precipitation.

ACKNOWLEDGEMENTS

The authors are grateful to Professor R.W. Cahn for provision of laboratory facilities and to Drs R.D. Doherty, J Perkins and S. Banerjee for fruitful discussion. We would also like to thank JEOL UK Ltd for the use of the JEOL 100C TEMSCAN Microscope. One of us (JJR) would like to acknowledge and thank the Science Research Council for the provision of a studentship and both authors would like to acknowledge the financial support of the US Office of Naval Research, (Grant number N-00014-78-G-0048).

REFERENCES

1. I.R. Sare and R.W.K. Honeycombe, Metal Science J., 1979, vol. 13, pp. 269-279.
2. A.T. Davenport, Ph.D. Thesis, Sheffield UK, 1968.
3. R.W. Cahn, K.D. Khrishnanand, M. Laridjani, M. Greenholz and R. Hill, Mat. Sci. & Eng., 1976, vol. 23, pp. 83-86.
4. F. Duflos, D.Phil. Thesis, Sussex, UK, 1980.
5. D.J. Dyson, S.R. Keown, D. Raynor and J.A. Whiteman, Acta Met, 1966, vol. 14, p. 867.
6. R. Wilson, "Metallurgy and Heat Treatment of Tool Steels", McGraw-Hill Book Co, London, 1975.
7. D. Raynor, J.A. Whiteman and R.W.K. Honeycombe, JISI, 1966, vol. 204, p. 1114.
8. A.K. Seal and R.W.K. Honeycombe, JISI, 1958, vol. 188, p.9.
9. I.R. Sare and R.W.K. Honeycombe, J. of Mat. Sci., 1978, vol. 13, pp. 1991-2002.
10. J.V. Wood and I.R. Sare, 'Proc. of 2nd Int. Conf. on Rapidly Quenched Metals' (ed. N.J. Grant and B.C. Giessen), 1976, vol. 1, pp. 87-94.
11. J.J. Rayment and B. Cantor, 'Proc. of 3rd Int. Conf. on Rapidly Quenched Metals', (ed. B. Cantor), vol. 1, pp. 85-93, The Metals Society, London, 1978.
12. J.J. Rayment, D.Phil. Thesis, Sussex, UK, 1979.
13. T. Arai and N. Komatsu, Tetsu-to-Hagane, 1972, vol. 58, p. 899.
14. T. Arai and N. Komatsu, Tetsu-to-Hagane, 1972, vol. 58, p. 1246.

15. J. Niewiarowski and H. Matyja, "Proc. of 3rd Int. Conf. on Rapidly Quenched Metals', (ed. B. Cantor), vol. 1, pp. 193-196, The Metals Society, London, 1978.

16. S.A.B. Jama and G. Thursfield, Tube Investments Research Laboratories, UK, Report No 322, 1972.

17. M. Tuli, P.R. Strutt, H. Nowotny and B.H. Kear, Proc. of 2nd Int. Conf. Rapid Solidification Processing, Reston, Virginia, USA, 1977.

18. P.R. Strutt, H. Nowotny, and B.H. Kear, 'Proc. of 3rd Int. Conf. Rapidly Quenched Metals', (ed. B. Cantor), vol. 1, pp. 171-175.

19. G. Hobson and D.S. Tyas, Metals & Materials, 1968, vol. 2, p. 144.

20. S. Takeda, Tech. Report of Tohoku Univ., 1931, vol. 10, p. 42.

21. P.G. Shewmon, "Diffusion In Solids", McGraw-Hill Book Co., New York, 1963.

22. J.T. Berry, High-Performance, High-Hardness High Speed Steels, Climas-Molybdenum, Greenwich, Conn. USA, 1970.

23. Y. Inokuti and B. Cantor, Scripta Met., 1976, vol. 10, p. 655.

24. P.G. Shewmon, "Transformations In Metals", McGraw-Hill Book Co., New York, 1969.

25. W. Hume-Rothery, "The Structures of Alloys In Iron", Pergamon Press, Oxford, 1966.

26. F. Duflos and B. Cantor, 'Proc. of 3rd Int. Conf. on Rapidly Quenched Metals', (ed. B. Cantor), vol. 1, pp. 110-118.

27. J.J. Rayment and B. Cantor, Met. Sci. J. 1978, vol. 12, p. 156.

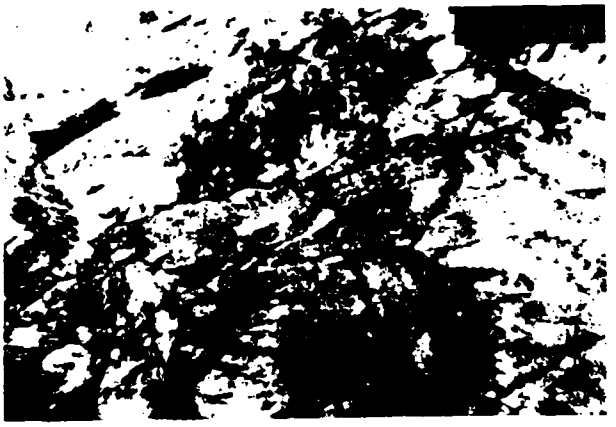

Fig 1 The martensitic lath microstructure of rapidly solidified FeWC1-3 alloys.

Fig 2a The microstructure of rapidly solidified FeWC4 alloy showing δ-ferrite cells surrounded by regions of austenite.

Fig 2b Area shown in Fig 2a, viewed in dark field using a $(110)_{\alpha}$ reflection.

Fig 2c Area shown in Fig 2a, viewed in dark field using a $(111)_{\gamma}$ reflection.

Fig 2d Selected area diffraction pattern of area shown in Fig 2a

Fig 3 The microstructure of rapidly solidified FeWC6 alloy, showing δ-ferrite cells surrounded by regions of austenite and M_6C carbide

Fig 4a The microstructure of rapidly solidified FeWC6 alloy

Fig 4b Area shown in Fig 4a, viewed in dark field using a $(242)_{M_6C}$ reflection.

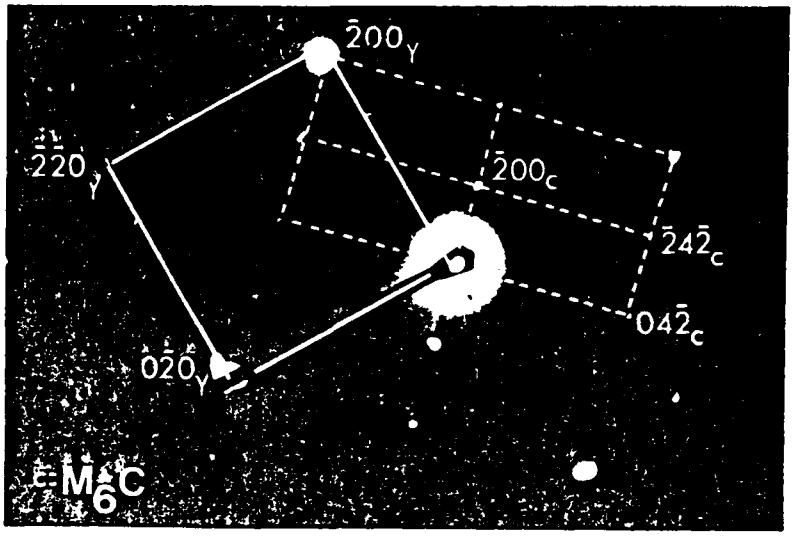

Fig 4c Selected area diffraction pattern of area shown in Fig 4a, containing an $[001]_\gamma$ zone and an $[012]_{M_6C}$ zone.

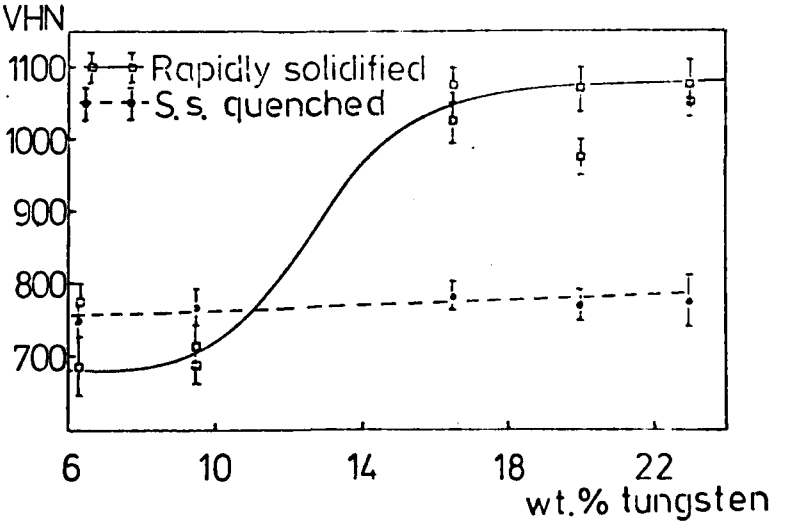

Fig 5 Microhardness of rapidly solidified and solid-state quenched Fe-W-C alloys as a function of tungsten content.

Fig 6 The microstructure of rapidly solidified T1 high speed tool steel, showing δ-ferrite cells surrounded by austenite and M_6C carbude.

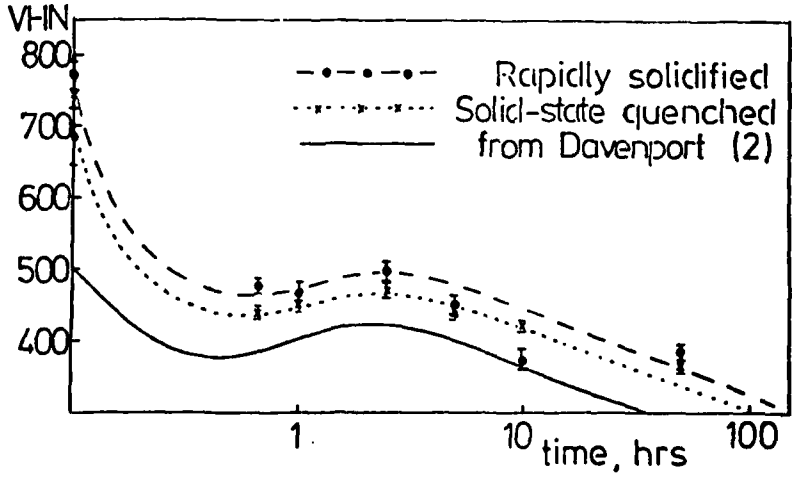

Fig 7 Microhardness as a function of tempering time at 600°C for rapidly solidified and solid-state quenched FeWC1 (6.3wt%W)

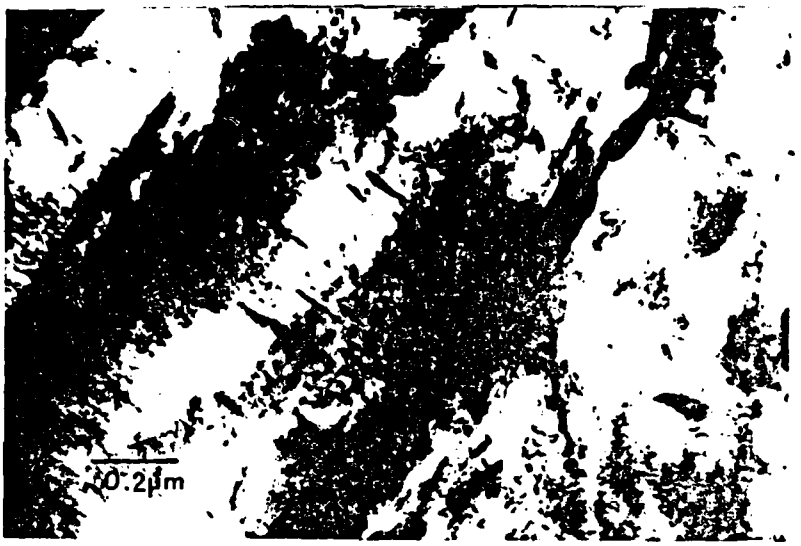

Fig 8 Rapidly solidified FeWCl tempered at 600°C for 40 minutes. Cementite has precipitated within the laths.

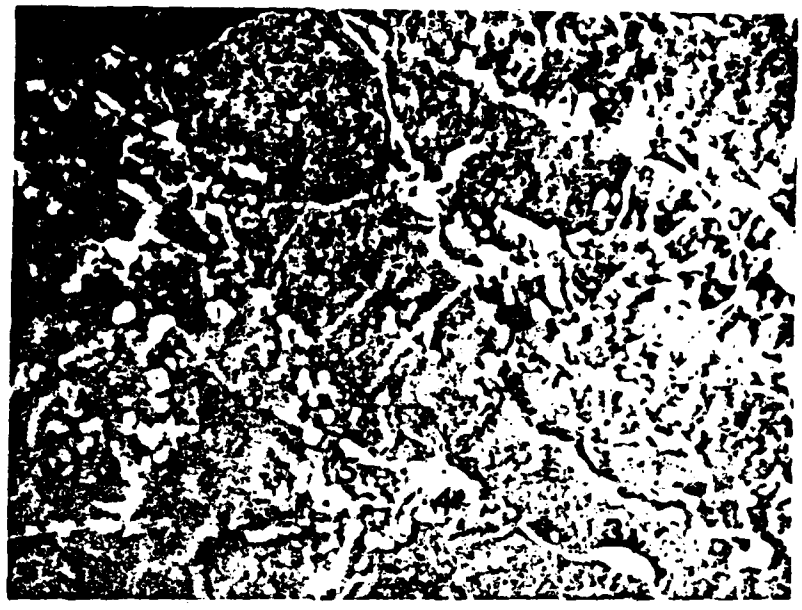

Fig 9a SEM micrograph of rapidly solidified FeWCl, tempered at 600°C for 10 hours.

Fig 9b STEM micrograph of rapidly solidified FeWCl, tempered at 600°C for 10 hours.

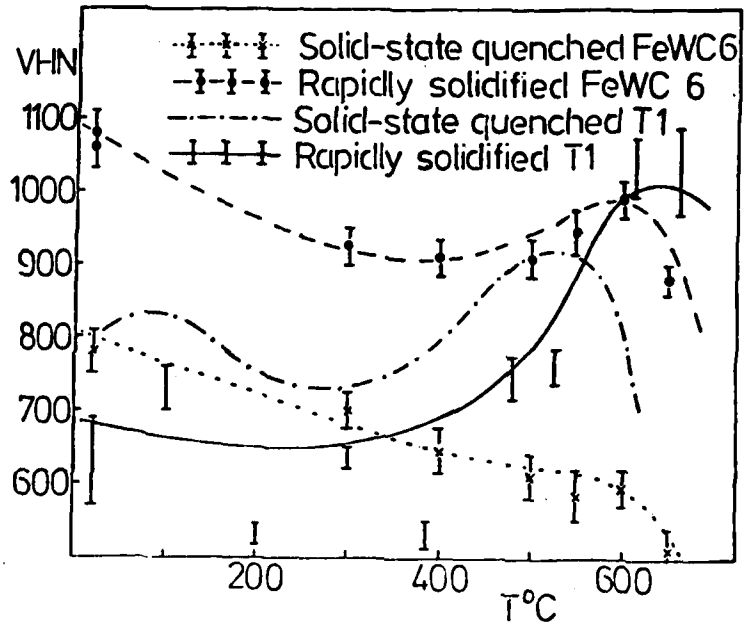

Fig 10 Microhardness as a function of tempering temperature for rapidly solidified and solid-state quenched FeWC6 alloy and T1 high speed tool steel.

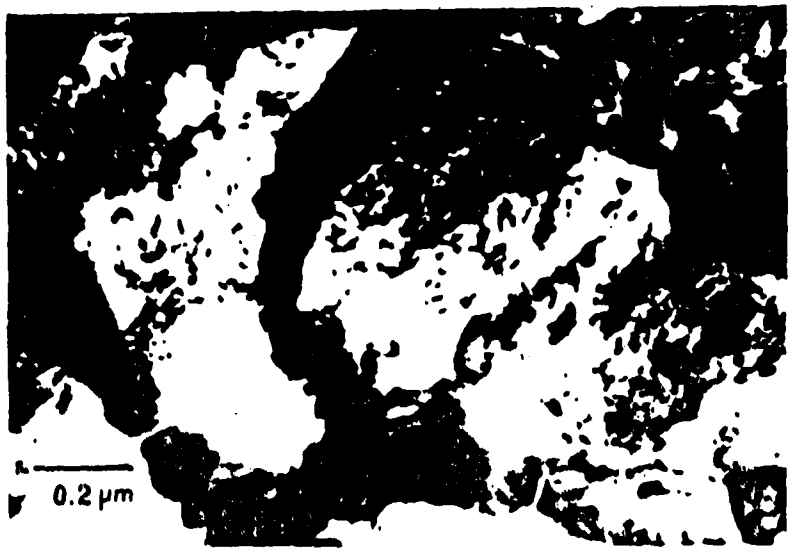

Fig 11 Rapidly solidified FeWC6 (23wt%W) tempered at 650°C for 1 hour. M_6C precipitation has occurred

Fig 12 Rapidly solidified T1 high speed tool steel tempered at 615°C for 1 hour. A fine precipitation of M_2C carbide has occurred within the δ-ferrite cells.

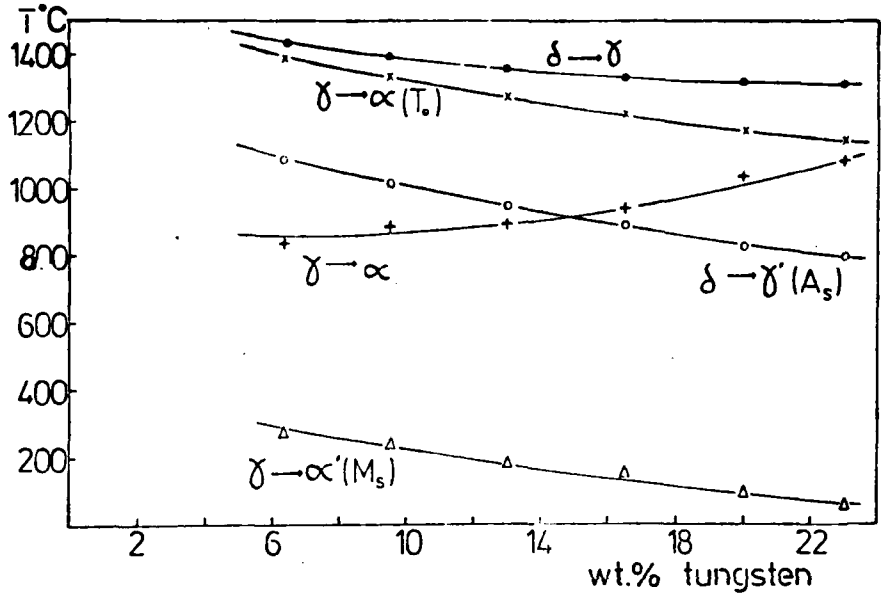

Fig 13 The transformation temperatures as a function of composition in rapidly solidified iron-tungsten-carbon alloys

ALLOY	Weight % of alloying element (atomic %)				
	W	C	V	Cr	Fe
FEWC 1	6.3 (1.99)	0.21 (0.99)	-	-	balance
FEWC 2	9.5 (3.05)	0.32 (1.53)	-	-	"
FEWC 3	13.0 (4.27)	0.42 (2.14)	-	-	"
FEWC 4	16.5 (5.54)	0.54 (2.77)	-	-	"
FEWC 5	20.0 (6.80)	0.65 (3.43)	-	-	"
FEWC 6	23.0 (8.06)	0.75 (4.03)	-	-	"
T1	18.0	0.75	1.10	4.0	"

Table I: Chemical compositions of six ternary Iron-tungsten-carbon alloys and commercial high speed tool steel T1.

AREA	1	2	3	4	5
Peak count	0.54	0.13	0.33	0.05	0.29
Integ. "	0.45	0.08	0.34	0.01	0.25
AREA	6	7	8	9	
Peak count	0.08	0.33	0.07	0.06	
Integ. "	0.05	0.31	0.03	0.04	

Table II: Peak counts and Integretated counts of the $\left[{}^{W}M\alpha \,/\, {}^{Fe}K\alpha \right]$ ratio for rapidly solidified Fe-6.3wt%W-0.21wt%C, tempered at 600^{o}C for 10 hours; Areas 1-7 are individual carbides and Areas 8-9 are within the matrix.

Authors	Tool Steel	i)Foil Thickness ii)Cooling Rate	Phases Present
Arai and Komatsu refs. 13,14	M2	i) 500-1500 μm	i) primary γ,eutectic γ+M_2C + MC ii)δ-ferrite,eutectic γ+M_2C + MC
Niewiarowski and Matyja ref.15	T1	i) 30-400 μm	bcc-iron, γ and M_6C
Jama and Thursfield ref.16	M2 and T1	i) ∿100 μm	δ-ferrite,γ (no carbide detected by optical microscopy)
Tuli et al. refs.17,18	T1	ii)∿$10^6 Ks^{-1}$	δ-ferrite, γ+ M_2C
Rayment and Cantor refs.11,12,27	M2,M42 and T1	i) 70-120 μm ii)∿$10^7 Ks^{-1}$	i) γ,bcc-iron,carbide -see refs 11,27 ii)δ-ferrite, γ+ M_6C -see ref12
Sare ref.1	M1	ii)∿10^6-$10^8 Ks^{-1}$	δ-ferrite, carbide (either M_2C,M_6C or $M_{23}C_6$)

Table III: The results of previous investigations into the effect of cooling rate on the rapidly solidified structures of high speed tool steels.

ALLOY	FeWC1	FeWC2	FeWC3	FeWC4	FeWC5	FeWC6	T1
Conventional	$L \rightarrow \delta$	$L \rightarrow \delta$	$L \rightarrow \delta$	$L \rightarrow \delta$	$L \rightarrow \delta$	$L \rightarrow \delta$	$L \rightarrow \delta$
Solidification	$L+\delta \rightarrow \gamma$	$L+\delta \rightarrow \gamma$	$L+\delta \rightarrow \gamma$	$L+\delta \rightarrow \gamma$	$L+\delta \rightarrow \gamma+M_6C$	$L+\delta \rightarrow \gamma+M_6C$	$L+\delta \rightarrow \gamma$
& Cooling	$\gamma_{sup} \rightarrow \gamma+M_6C$	$\gamma_{sup} \rightarrow \gamma+M_6C$	$L \rightarrow \gamma+M_6C$	$L \rightarrow \gamma+M_6C$	$\gamma \rightarrow \alpha$	$\gamma \rightarrow \alpha'$	$L \rightarrow \gamma+M_6C$
Sequences	$\gamma \rightarrow \alpha'$	$\gamma \rightarrow \alpha'$	$\gamma \rightarrow \alpha'$	$\gamma \rightarrow \alpha'$			$\delta \rightarrow \gamma+M_6C$
							$\gamma \rightarrow \alpha'$
Rapid	$L \rightarrow \delta$	$L \rightarrow \delta$	$L \rightarrow \delta$	$L \rightarrow \delta$	$L \rightarrow \delta$	$L \rightarrow \delta$	$L \rightarrow \delta$
Solidification	$L+\delta \rightarrow \gamma$	$L+\delta \rightarrow \gamma$	$L+\delta \rightarrow \gamma$	$L+\delta \rightarrow \gamma$	$L+\delta \rightarrow \gamma+M_6C$	$L+\delta \rightarrow \gamma+M_6C$	$L+\delta \rightarrow \gamma+M_6C$
Sequence	$\delta \rightarrow \gamma$	$\delta \rightarrow \gamma$	$\delta \rightarrow \gamma$				
	$\gamma \rightarrow \alpha''$	$\gamma \rightarrow \alpha''$	$\gamma \rightarrow \alpha''$				

Table IV: The conventional solidification and cooling sequences and the rapid solidification and cooling sequences for the six iron-tungsten-carbon alloys and T1 highspeed tool steel.

ALLOY	D, $cm^2 sec^{-1}$	Time, sec.	$X = \sqrt{Dt}$, μm
FEWC 1	6.02×10^{-6}	2.4×10^{-4}	0.38
FEWC 2	6.80×10^{-6}	2.0×10^{-4}	0.37
FEWC 3	6.40×10^{-6}	1.9×10^{-4}	0.34
FEWC 4	6.80×10^{-6}	1.7×10^{-4}	0.34
FEWC 5	8.30×10^{-6}	1.4×10^{-4}	0.34
FEWC 6	1.02×10^{-5}	1.0×10^{-4}	0.32
T1	6.50×10^{-6}	1.9×10^{-4}	0.35

Table V : The diffusion of carbon in δ-ferrite in rapidly solidified Iron-tungsten-carbon alloys and T1 high speed steel.

ALLOY	D, cm^2 sec^{-1}	Time, sec.	X= $/\overline{Dt}$ μm
FEWC 1	3.95×10^{-9}	2.4×10^{-4}	0.97×10^{-2}
FEWC 2	6.20×10^{-9}	2.0×10^{-4}	1.11×10^{-2}
FEWC 3	4.90×10^{-9}	1.9×10^{-4}	0.96×10^{-2}
FEWC 4	6.20×10^{-9}	1.7×10^{-4}	1.03×10^{-2}
FEWC 5	1.32×10^{-8}	$1\ 4 \times 10^{-4}$	1.35×10^{-2}
FEWC 6	1.74×10^{-8}	1.0×10^{-4}	1.32×10^{-2}
T1	4.90×10^{-9}	1.92×10^{-4}	0.97×10^{-2}

Table VI: The diffusion of tungsten in δ-ferrite in rapidly solidified Iron-tungsten-carbon alloys and T1 high speed steel .